

# Boosting of Purcell Enhancement Factor near Exceptional Point Degeneracies in an Elastodynamic Metamaterial

Abhishek Gupta<sup>1</sup>, Arkady Kurnosov<sup>2</sup>, Tsampikos Kottos<sup>2,#</sup>, Ramathasan Thevamaran<sup>1,3,\*</sup>

<sup>1</sup>Department of Mechanical Engineering, University of Wisconsin Madison; Madison, Wisconsin, 53706, USA.

<sup>2</sup>Wave Transport in Complex Systems Lab, Physics Department, Wesleyan University; Middletown, CT-06459, USA.

<sup>3</sup>Department of Engineering Physics, University of Wisconsin Madison; Madison, Wisconsin, 53706, USA.

Corresponding authors: # [tkottos@wesleyan.edu](mailto:tkottos@wesleyan.edu) , \* [thevamaran@wisc.edu](mailto:thevamaran@wisc.edu)

**Abstract:** The Purcell emissivity enhancement of a quantum source due to its surrounding environment is intimately related to the Fermi's Golden Rule (FGR) which connects the emission rate of a source with the Local Density of States (LDoS) of the environment. Such viewpoint extends the applicability of Purcell enhancement to other areas, ranging from electromagnetics to acoustics and mechanical waves, where the LDoS of the environment can favorably be tailored. Here, we utilize this viewpoint in designing an elastodynamic metamaterial which supports an exceptional point degeneracy (EPD) and experimentally show that when it is coupled to an actuation source it boosts the Purcell enhancement factor beyond its expected value while maintaining a constant signal quality. On the technological front, our proof-of-principle metamaterial system promotes a new class of nano-indenters and robotic-actuators while at the fundamentals, it allows for a deeper understanding of the ramifications of EPDs in the applicability of FGR and Purcell physics.

The unveiled wealth of underlying mathematical structures of the non-Hermitian wave systems [1,2] and their utilization in new technologies have flourished over the last few years. The non-Hermitian notions have influenced various areas of physics such as optics and photonics [3,4], RF and microwaves [5–7], optomechanics [8], acoustics [9,10], physics of cold atoms [11], magnonics [12,13], and most recently elastodynamics [14–17]. Consequently, new concepts have been developed and realized in these frameworks. Examples include a loss-induced transparency [18], unidirectional invisibility [19], parity-time-symmetric lasers [20,21], hypersensitive sensors [22–25], etc. Many of these phenomena are reliant on the existence of EPDs. Their implementation requires judicious design of attenuation (and/or amplification) and impedance profiles that lead to enhanced wave-matter interactions.

As opposed to many of these previous studies that emphasized the topology of the eigenfrequency surfaces in the parameter space near an EPD, here we exploit *phenomena intimately related to the eigenvector coalescence at EPDs* [2] and its ramifications in the shape of the Local Density of States (LDoS). The latter has been recently attracted a lot of attention in the optics framework [26–32]. Specifically, it was theoretically argued that a direct consequence of

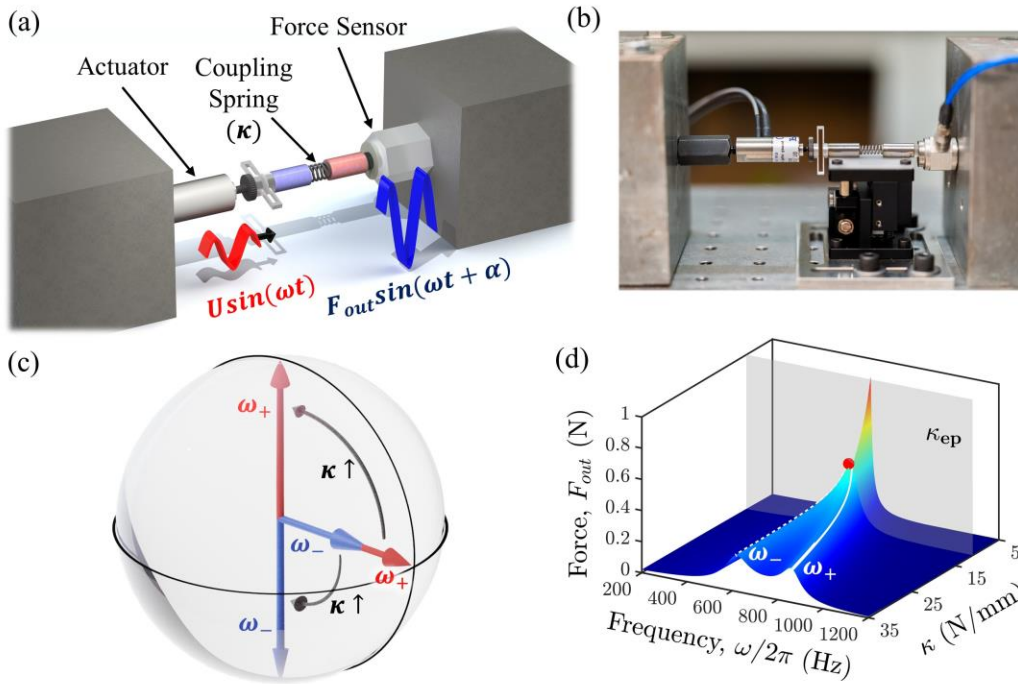


**FIG. 1. Actuation force enhancement by exploiting eigenvector degeneracies.** (a) A schematic and (b) a photograph of the experimental setup used in this study showing a non-Hermitian metamaterial consisting of two coupled resonators with one made of a Hookean aluminum spring and the other made of a viscoelastic material (PDMS) with controlled crosslinking. This metamaterial is mounted between a piezoelectric actuator and a dynamic force sensor with an applied static precompression and supported by a low-friction Teflon surface mount. A frequency sweep is performed by applying a sinusoidal displacement excitation  $U \cdot \sin(\omega t)$  ( $U$  is amplitude and  $\omega$  is frequency) on the left side (undamped resonator/mass). The exerted force  $F_{out} \sin(\omega t + \alpha)$ , ( $F_{out}$  is force amplitude and  $\alpha$  is phase lag) is measured on the right side for various coupling spring stiffnesses ( $\kappa$ ). (c) The eigenmodes of the non-Hermitian system are skewed and become degenerate at the exceptional point corresponding to a critical coupling  $\kappa = \kappa_{EP}$ . (d) Theoretically predicted reaction force amplitude as a function of excitation frequency ( $\omega$ ) and coupling ( $\kappa$ ). The force exerted on the force sensor is twice as large in the proximity of the EPD as compared to when metamaterial is operating away from the EPD, i.e., with higher coupling spring stiffness ( $\kappa \gg \kappa_{EP}$ ).

such eigenbasis collapse is an anomalous emissivity enhancement of a source when it is brought at the proximity of an environment (e.g. a cavity) featuring EPDs. The underlying physics of emissivity enhancement of a source due to a surrounding environment is known as Purcell effect and has been initially developed in the framework of quantum electrodynamics [33]. It described the modification of the spontaneous emission rate of a quantum source by changing its environment via manipulation of the local density of states (LDoS) of the quantum system. The latter information is imprinted in the Green’s function that describes the surrounding environment. Interestingly, this same physics is intimately connected with one of the most fundamental rules of quantum mechanics: The Fermi’s Golden Rule (FGR) [34] which links emission rates to the LDoS of the system. Elucidating the Purcell physics from this angle allows for expanding its applications to various wave systems where cavity manipulation can be employed to tailor the LDoS of the environment to which a source is coupled. Purcell effect has benefitted numerous technologies such as nano-optical spectroscopy, nanolasing, quantum information processing, energy harvesting, emission enhancement of sound and elastodynamic sources, etc [35–44]. An investigation, therefore, of non-Hermiticity and EPDs and their ramifications in FGR and Purcell physics constitutes a dual benefit: on a fundamental level, it will provide us a deeper understanding of the connection between engineered impedance and one of the basic rules, i.e., FGR, while on the technological level, it will allow us to exploit the effects of non-Hermitian spectral singularities like EPDs to enhance the emissivity of mechanical sources.

To this end, we have designed a two-mode cavity (the “environment” in the Purcell-physics framework) made by a non-Hermitian elastodynamic metamaterial consisting of two coupled resonant elements with differential damping between them [Fig. 1(a) and 1 (b)]. The damped ( $m_2 = m = 4.635 \text{ gm}$ ) and the undamped ( $m_1 = m$ ) resonators (masses) are coupled by a coiled Hookean spring of stiffness  $\kappa$ , see Figs. 1(a) and 1(b). When the Hookean coupling strength between the two resonators acquires a critical value, the system exhibits an EPD associated with a coalescence of its eigenmodes (Fig. 1(c)) and the corresponding eigenfrequencies (Fig. 1(d)). Beyond this critical coupling, the eigenfrequencies bifurcate into two resonant modes with approximately the same constant linewidths. In this domain, a constant-amplitude dynamic force (the “source” in the Purcell framework) applied on the undamped resonator side (the “dark” mode) of the metamaterial results in an actuation force—i.e., the force exerted by the damped resonator (the “bright” mode) side of the metamaterial onto the dynamic force sensor—whose amplitude is controlled by the coupling strength between the two masses without any deterioration of force-signal quality. The actuation force is enhanced by 6.4 times at the proximity of an EPD compared to the 3.2 times enhancement produced by the same cavity-source system when the metamaterial does not support an EPD, see Fig. 1(d) and Supplementary material [45]. Conventional Purcell physics cannot explain this phenomenon—twice as large enhancement near an EPD. Its origin is traced back to the coalescence of the dark (small decay rates) and bright (large decay rates) resonances supported by the undamped and damped resonators, respectively. Consequently, an excitation source (emitter) on resonance with a dark mode can deliver on the other end an actuation force only if it is coupled to a leaky resonance. Such a shared resonance underlies the enhancement near the EPD. It is reflected in a narrowing of the Green’s function that describes the metamaterial—and consequently its LDoS—which acquires a square Lorentzian line-shape whose peak has a fourfold enhancement with respect to the peak of a single resonance. Our proof-of-principle metamaterial system promotes a new class of nano-indenters, atomic force microscopes and robotic-actuators.

To achieve differential damping between the two resonant elements of the metamaterial, we have designed and fabricated two types of springs: a compliant aluminum spring with

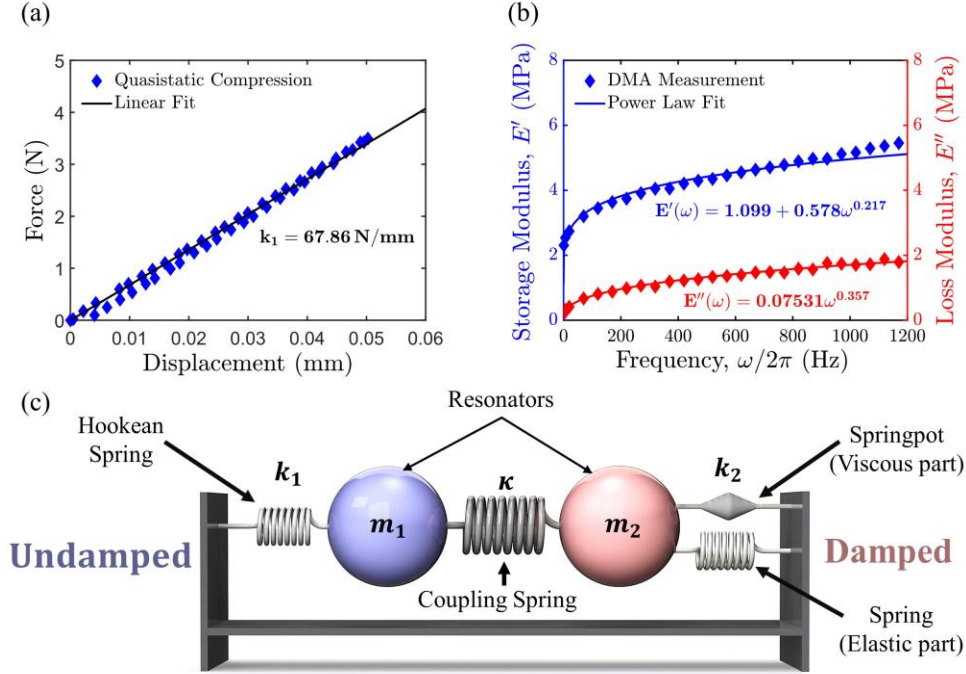


**FIG. 2. The design of non-Hermitian metamaterial.** (a) Force vs. Displacement of the compliant aluminum Hookean spring ( $F = k_1 x_1$ ). (b) Dynamic mechanical analysis (DMA) of frequency-dependent storage and loss moduli of PDMS and corresponding power law fits. (c) Conceptual design of non-Hermitian coupled resonators with differential damping. Viscoelastic material (damped component) is represented by a parallel combination of an elastic spring and a springpot, where  $k_2$  is the complex dynamic stiffness of the viscoelastic material. Undamped component is represented by a Hookean spring of stiffness  $k_1$ . Damped and undamped components are coupled together by a coiled spring of spring constant  $\kappa$ .

specifically designed stiffness for the undamped component and a viscoelastic poly(dimethylsiloxane) (PDMS) for the damped component (see Figs. 1(a) and 1(b)). For the undamped component, we fabricated a lightweight aluminum spring (T6-6061), whose geometry was designed using finite element modeling such that the spring does not yield plastically under static pre-stress. Its effective stiffness allows for an EPD to form as we vary the coupling between the two elements. Quasistatic and dynamic mechanical analysis of the aluminum spring (Fig. 2(a)) indicates that it follows Hooke's law with a spring constant  $k_1 = 67.86 \text{ N/mm}$  as designed, resulting in a natural frequency of  $\omega_0 = \sqrt{k_1/m} \approx 609 \text{ Hz}$  for the undamped resonator. We fabricated the PDMS films with different amounts of crosslinking, which was controlled by varying the percentage of the curing-agent (5 to 10% wt.) to tailor its dynamic modulus and loss-tangent. Then, 6 mm diameter cylindrical specimens were cutout and preconditioned through five quasistatic compressive loading-unloading cycles up to 30% strain to remove any potential variations in the constitutive response of the pristine material. We used an optimal cylindrical specimen—a softer PDMS with large loss-tangent identified from the material's storage and loss moduli measured by dynamic mechanical analysis (DMA)—as the damped spring component of the metamaterial. The DMA was performed by first applying a 10% static precompression strain to the cylindrical PDMS specimens and then harmonically exciting them with a piezoelectric actuator (Physik Instrumente P841.10) at prescribed strain amplitudes and at frequencies ranging

from 1 Hz to 1200 Hz while measuring the response force by a dynamic force sensor (PCB 208C01). The measured amplitude and phase lag between the actuation and the dynamic force signal were then used to calculate the frequency-dependent storage ( $E'(\omega)$ ) and loss ( $E''(\omega)$ ) moduli. The measured storage and loss moduli were then fitted using power-law functions (see Fig. 2(b)). The fits were used for the numerical modeling as well as the design of the metamaterial.

We model the dynamics of the metamaterial by the following integro-differential equations

$$m_1 \ddot{x}_1 = -k_1(x_1 - x_0(t)) - \kappa(x_1 - x_2) \quad (1a)$$

$$m_2 \ddot{x}_2 = -\sigma(t)A - \kappa(x_2 - x_1) \quad (1b)$$

describing two coupled masses ( $m_1, m_2$ ) with displacements ( $x_1(t), x_2(t)$ ) respectively, see Fig. 2(c). The Hookean spring constant of the aluminum spring is  $k_1$ , and  $x_0(t) = U \cdot \sin(\omega t)$  is the displacement prescribed by the actuator, while  $F_{out} = -\sigma(t)A$  is the force exerted on the mass  $m_2$  with  $A (= 28.274 \text{ mm}^2)$  and  $\sigma(t)$  being the cross-sectional area and the stress response of the PDMS specimen respectively. In the frequency domain, Eqs. (1) take the form

$$-m\omega^2 x_1 + k_1 x_1 + \kappa(x_1 - x_2) = k_1 U \quad (2a)$$

$$-m\omega^2 x_2 + \kappa(x_2 - x_1) + k_2(\omega)x_2 = 0 \quad (2b)$$

where  $k_2(\omega) \equiv (A/h) \left( \frac{\sigma(\omega)}{\epsilon(\omega)} \right)$  is the dynamic stiffness of the PDMS with  $\epsilon(\omega) = x_2(\omega)/h$  being the Fourier transform of the strain, and  $h (= 1.948 \text{ mm})$  is the thickness of the PDMS specimen. The stress amplitude is commonly expressed in terms of storage ( $E'$ ) and loss ( $E''$ ) moduli and strain ( $\epsilon$ ) as  $\sigma(\omega) = [E'(\omega) + iE''(\omega)]\epsilon(\omega)$ .

The corresponding eigenfrequencies  $\omega_{\pm}$  of the metamaterial are found by solving the characteristic equation associated with Eq. (2). Figs. 3(a) and 3(b) show the real and imaginary parts of  $\omega_{\pm}$  as functions of the stiffness  $\kappa$  of the coiled coupling spring. It turns out that at a critical coupling  $\kappa_{EP}$ , they lead to an EPD corresponding to a resonant frequency  $\omega_- = \omega_+ = \omega_{EP}$ . As the coupling stiffness  $\kappa$  is increased above  $\kappa_{EP}$  the modes separate from one another, i.e.  $\omega_-^R \equiv \text{Re}(\omega_-) \neq \text{Re}(\omega_+) \equiv \omega_+^R$ , while their linewidths remain approximately the same, i.e.  $\omega_-^I \equiv \text{Im}(\omega_-) \approx \text{Im}(\omega_+) \equiv \omega_+^I$  (see Methods). Our modeling is further validated by a direct comparison with the measured eigenvalues (see Methods), see Figs. 3(a) and 3(b).

We further evaluate the mechanical power dissipated from mass  $m_2$ , which takes the form (see Methods)

$$P_d(\omega) = \frac{\omega}{2\pi} W_d = \Phi_e \cdot \xi(\omega) \quad \text{where} \quad \xi(\omega) = \frac{2\omega}{\pi} \text{Im}G_{11}(\omega) \quad (3)$$

where  $W_d(\omega) = Ah \int_0^{2\pi/\omega} dt \sigma(t) \frac{d\epsilon}{dt} = (\pi Ah) E''(\omega) |\epsilon(\omega)|^2$  is the dissipated energy per cycle [46],  $\Phi_e = \frac{\pi F_{in}^2}{4m}$  depends only on the equivalent input force from the actuator  $F_{in} = k_1 U$  acting on the mass  $m_1 = m$ , and  $G_{11}(\omega)$  is the element of the Green's function that describes the system of Eq. (2)

The Eq. (3) establishes a connection between the power dissipated by the elastodynamic metamaterial shown in Figs. 1(a) and 1(b) and the Purcell physics of quantum optics. The analogies become clearer once we interpret the imaginary part of the Green's function  $\xi(\omega)$  as the LDoS of the mechanical resonant cavity formed by the metamaterial, and the piezoelectric actuator that excites the system as an emitter placed in the proximity of this cavity. Then the mechanical power emitted by the metamaterial is the analogue of the emissive power in the quantum optics framework. In the latter framework, Purcell realized that the spontaneous emission rate of a quantum emitter is enhanced (or suppressed) by appropriately engineering its surrounding environment, and therefore, the LDoS [33].

Further theoretical progress can be made by assuming that the storage and loss moduli take a constant value in the frequency range of our experiments which are  $E' = \frac{k_1 h}{A} = 4.675 \text{MPa}$  and  $E'' = 1.5235 \text{MPa}$  (see Methods). This approximation is justified by the slow frequency dependence that the PDMS exhibits, see Fig. 2(b). Under this approximation, the critical coupling is  $\kappa_{EP} = \frac{A}{2h} E''$ , and for  $\kappa \geq \kappa_{EP}$  the two resonant modes exhibit approximately the same decay rate  $2\omega_{\pm}^I \approx \Gamma \equiv \frac{A}{2mh\omega_0} E''$  (see Fig. 3(b)). In this case  $\xi(\omega)$  becomes

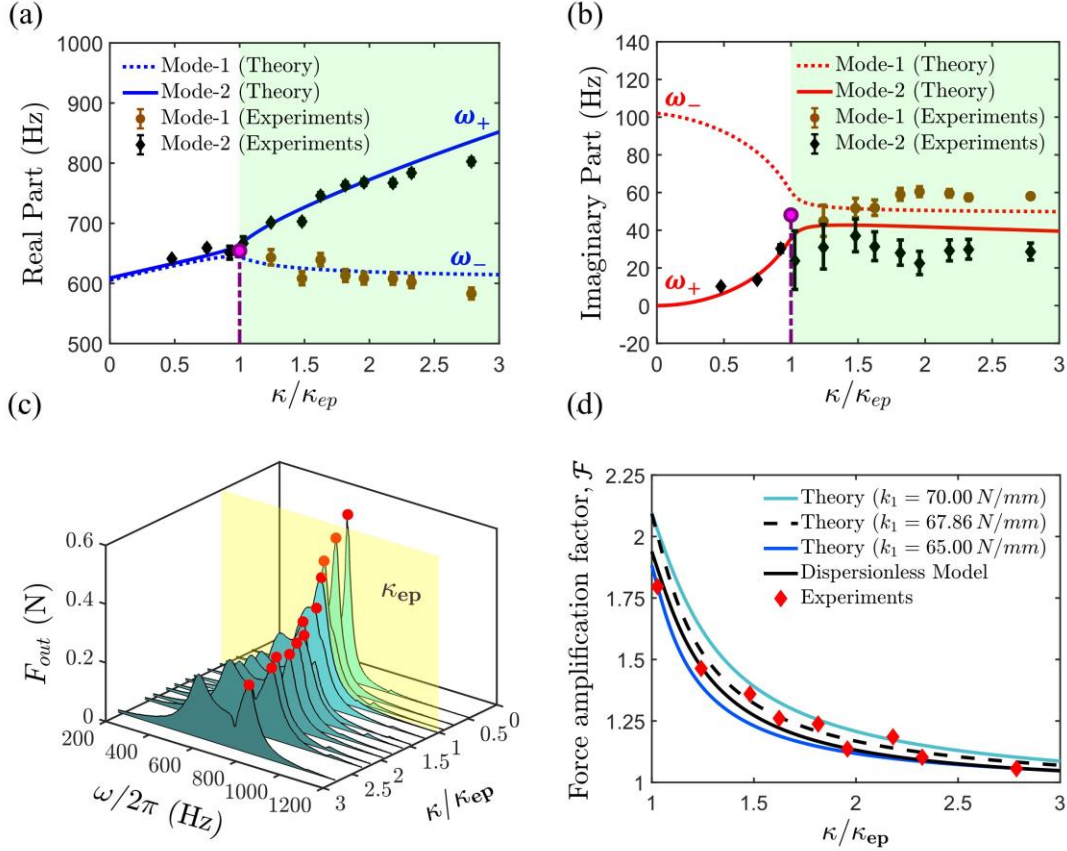


**FIG. 3. Theoretical and experimental demonstration of the actuation force enhancement by the non-Hermitian metamaterial.** (a) The real and (b) the imaginary parts of resonant frequencies ( $\omega_{\pm}$ ) vs. coupling strength, obtained by a modal curve-fitting of the experimentally measured force spectra. The solid and dotted lines are the results of the simulations with the model described by Eq. (2) where dispersion effects are considered. The Hookean spring constant was taken to be  $k_1 = 67.86 \text{kN/m}$ . (c) Frequency-swept force amplitude measured experimentally for various coupling spring stiffnesses. Splitting of a single sharp peak into two broad peaks can be observed as coupling increases. (d) Emitted force amplification factor  $\mathcal{F}(\omega_{\pm})$  vs the rescaled coupling. The experimental data are indicated in filled diamonds. The solid black line indicates the results of the dispersionless modeling with  $k_1 = 70 \text{kN/m}$ . Solid lines indicate the results of the simulations of model Eq. (2) for three different  $k_1$ -values corresponding best fitting  $k_1 = 67.86 \text{N/mm}$  (black dash line) and  $k_1 = 70 \text{N/mm}$  and  $k_1 = 65 \text{N/mm}$  representing the uncertainty in the data fitting of Fig. 2(a). A two-fold enhancement is observed in all cases.

$$\xi(\omega) = \frac{1}{\pi} \frac{\Gamma \cdot \omega_0 \cdot (\kappa/m)^2 \omega}{(\omega^2 - \omega_0^2)^2 (\omega^2 - \omega_0^2 - 2\kappa/m)^2 + (2\Gamma\omega_0)^2 (\omega^2 - \omega_0^2 - \kappa/m)^2} \quad (4)$$

where  $\omega_0 = \sqrt{k_1/m}$ . Because at the proximity of the EPD the two eigenfrequencies degenerate at  $\omega_{\pm}^R = \omega_{EP} \approx \omega_0 \sqrt{1 + \Gamma/\omega_0} \approx \omega_0$  (see Methods), one naturally expects that  $\xi(\omega)$ , and subsequently  $P_d(\omega)$ , will also be modified. To better understand the consequence of EPD on them, we first evaluate  $\xi(\omega)$  in the vicinity of  $\omega \approx \omega_{EP}$ . From Eq. (4), we get that (see Supplementary Material [45])

$$\xi_{EP}(\omega) \approx \frac{1}{2\pi} \frac{(\Gamma/2)^3}{[(\omega - \omega_{EP})^2 + (\Gamma/2)^2]^2} \quad (5)$$

corresponding to a square-Lorentzian—as opposed to the more traditional Lorentzian line-shape characterizing the LDoS away from an EPD. In the other limiting case of  $\kappa \gg \kappa_{EP}$ , the two resonant frequencies  $\omega_{-}^R \approx \omega_0$  and  $\omega_{+}^R \approx \sqrt{\omega_0^2 + (2\kappa/m)}$  (see Methods) are well separated from each other. In this case one can approximate Eq. (4) as a sum of two Lorentzians centered at  $\omega_{\pm}$  and having the same linewidth  $\Gamma$ . Specifically, we have

$$\xi_{\infty}(\omega) \approx \frac{1}{8\pi} \sum_{\pm} \frac{\Gamma/2}{(\omega - \omega_{\pm}^R)^2 + (\Gamma/2)^2} \quad (6)$$

which can be used as a reference for measuring the effects of EPD in the power emission. At this point, it is instructive to introduce the rescaled dissipated power  $\mathcal{P}(\omega_e) = P_d(\omega_e)/P_d^{\infty}(\omega_{\pm}^R)$  where  $P_d^{\infty}(\omega_{\pm}) \equiv \frac{\pi}{2} \Phi_e \cdot \xi_{\infty}(\omega_{\pm})$  and  $\omega_e = \omega_{\pm}^R$  is the frequency of the actuation force which is considered to be monochromatic and at resonant frequency. Substituting Eqs. (5) and (6) back in the general expression for the emissivity Eq. (3), we deduce that  $\mathcal{P}(\omega_e = \omega_{EP}) = 4$ . It is important to emphasize that the four-fold enhancement is a consequence of EPDs involving dark and bright resonances and sources that couple only to the dark resonant mode. An intuitive understanding is gained by realizing that, even though the underlying coupled resonances exhibit the same asymptotic decay rates at EPD, the source is allowed to directly probe the infinite lifetime of the dark resonance. A more careful analysis (see Supplementary Material [45]) indicates that  $\mathcal{P}(\omega_e = \omega_{EP})$  might be slightly larger/smaller than a factor of four, i.e.,  $\mathcal{P}(\omega_e = \omega_{EP}) \approx 4 + \mathcal{O}\left(\frac{\Gamma}{\omega_0}\right) + \mathcal{O}\left(\frac{\kappa}{k_1}\right)$ , where  $\frac{\Gamma}{\omega_0} \ll 1$ ;  $\frac{\kappa}{k_1} < 1$ .

The enhanced dissipated power due to the four-fold enhancement of the peak of  $\xi(\omega)$  is also reflected in the actuation force emitted from the metamaterial and measured by the dynamic force sensor attached to the  $m_2$ -resonator. The latter is written in the form  $F_{out}(t) = F_{out}(\omega_e) \sin(\omega_e t + \alpha)$ , where  $\omega_e$  is the driving frequency of the actuator. At the same time, the emitted force amplitude  $|F_{out}(\omega_e)|$  is

$$|F_{out}(\omega_e)| \equiv A|\sigma(\omega_e)| = \sqrt{\frac{2A(|E'(\omega_e)|^2 + |E''(\omega_e)|^2)}{h\omega_e E''(\omega_e)}} P_d(\omega_e), \quad (7)$$

where we have expressed the stress function as  $\sigma(\omega) = [E'(\omega) + iE''(\omega)]\epsilon(\omega)$  and subsequently we have used Eq. (3) to express the strain in terms of the emitted power as  $|\epsilon(\omega)| = \sqrt{4P_d(\omega)/(\pi E'' A h)}$ . From Eq. (7) we can further estimate the force amplification factor  $\mathcal{F}(\omega_e) \equiv \frac{F_{out}(\omega_e)}{F_{out}^{\infty}(\omega_{\pm}^R)} = \sqrt{\mathcal{P}(\omega_e)}$ , which for  $\kappa_{EP}$  and driving frequency  $\omega_e = \omega_{EP}$  is  $\mathcal{F}(\omega_e = \omega_{EP}) = 2$ . We point out that the force amplification factor  $\mathcal{F}(\omega_e)$  indicates an additional enhancement relative to

the typical Purcell force enhancement occurring in the actuating force  $F_{out}^{\infty}(\omega_{\pm}^R)$  for the same metamaterial-source configuration when the metamaterial does not support an EPD.

We have tested the validity of the above predictions by direct measurements of the emitted actuation force amplitude (Fig. 3(c)) for various coupling stiffness  $\kappa$  versus the driving frequency  $\omega_e$  (see Methods). From these data we extracted the force amplification factor  $\mathcal{F}(\omega_e = \omega_{\pm})$  and report it as a function of the coupling stiffness  $\kappa$  normalized by the coupling stiffness corresponding to the EPD,  $\kappa_{EP}$ , in Fig. 3(d). The experimental data confirm the above theoretical predictions very well. In the same figure, we also report the force amplification factor calculated numerically from Eqs. (2). From these equations, we extracted the frequency-dependent displacement amplitude  $x_2(\omega)$  using the dispersion characteristics of the stress function, which is related to the strain in viscoelastic material as  $\epsilon(\omega) = x_2(\omega)/h$ . Using the definition of  $|F_{out}(\omega)|$  in Eq. (7), we have calculated  $\mathcal{F}(\omega_e = \omega_{\pm}^R)$  for three different  $k_1$  constants to evaluate the robustness of the observed two-fold enhancement. In the same figure, we also report the theoretical results of the non-dispersive model (solid black line). All curves confirm the two-fold enhancement in actuation force at the proximity of the EPD with respect to the actuation force value corresponding to large coupling constants where a standard cavity-enhancement Purcell effect occurs.

In conclusion, we have demonstrated experimentally and analyzed theoretically an enhancement in the exerted actuation force and the emitted mechanical power by a bright resonance mode of a non-Hermitian elastodynamic cavity—a metamaterial consisting of two modes—when its pair dark resonance mode is excited directly by an actuation source. The origin of this enhancement has been traced to the reorganization of the super-modes of the metamaterial in the proximity of an EPD. Our experiments pave the way for understanding the ramifications of non-Hermiticity and EPD engineering in the manipulation of the Purcell factor of narrow-band emitters. It also provides a unique metamaterial design pathway that exploits differential damping to control its effective dynamics and modification of its surrounding environment via a source that is specifically coupled to a local element of the metamaterial for achieving an actuation force enhancement while maintaining a constant quality factor of the dynamics. It can also be used as a proof-of-principle design of a novel class of indenters for material hardness measurements [47] or for enhanced reconfigurable actuations in robotics.

## References

- [1] C. M. Bender, *Making Sense of Non-Hermitian Hamiltonians*, Reports on Progress in Physics **70**, 947 (2007).
- [2] T. Kato, *Perturbation Theory for Linear Operators* (Springer Berlin / Heidelberg, 1995).
- [3] R. El-Ganainy, K. Makris, M. Khajavikhan, Z. Musslimani, S. Rotter, and D. Christodoulides, *Non-Hermitian Physics and PT Symmetry*, Nature Physics **14**, (2018).
- [4] M.-A. Miri and A. Alù, *Exceptional Points in Optics and Photonics*, Science (1979) **363**, eaar7709 (2019).
- [5] R. Thomas, H. Li, F. M. Ellis, and T. Kottos, *Giant Nonreciprocity near Exceptional-Point Degeneracies*, Phys. Rev. A **94**, 43829 (2016).
- [6] J. Doppler, A. A. Mailybaev, J. Böhm, U. Kuhl, A. Girschik, F. Libisch, T. J. Milburn, P. Rabl, N. Moiseyev, and S. Rotter, *Dynamically Encircling an Exceptional Point for Asymmetric Mode Switching*, Nature **537**, 76 (2016).
- [7] S. Assaworarith, X. Yu, and S. Fan, *Robust Wireless Power Transfer Using a Nonlinear Parity-Time-Symmetric Circuit*, Nature **546**, 387 (2017).
- [8] H. Xu, D. Mason, L. Jiang, and J. G. E. Harris, *Topological Energy Transfer in an Optomechanical System with Exceptional Points*, Nature **537**, 80 (2016).
- [9] C. Shi, M. Dubois, Y. Chen, L. Cheng, H. Ramezani, Y. Wang, and X. Zhang, *Accessing the Exceptional Points of Parity-Time Symmetric Acoustics*, Nat. Commun. **7**, 11110 (2016).

- [10] R. Thevamaran, R. M. Branscomb, E. Makri, P. Anzel, D. Christodoulides, T. Kottos, and E. L. Thomas, *Asymmetric Acoustic Energy Transport in Non-Hermitian Metamaterials*, *J. Acoust. Soc. Am.* **863**, (2019).
- [11] P. Peng, W. Cao, C. Shen, W. Qu, J. Wen, L. Jiang, and Y. Xiao, *Anti-Parity-Time Symmetry with Flying Atoms*, *Nature Physics* **12**, (2016).
- [12] J. M. Lee, T. Kottos, and B. Shapiro, *Macroscopic Magnetic Structures with Balanced Gain and Loss*, *Phys. Rev. B* **91**, 94416 (2015).
- [13] D. Zhang, X. Q. Luo, Y. P. Wang, T. F. Li, and J. Q. You, *Observation of the Exceptional Point in Cavity Magnon-Polaritons*, *Nature Communications* **8**, (2017).
- [14] V. Domínguez-Rocha, R. Thevamaran, F. M. Ellis, and T. Kottos, *Environmentally Induced Exceptional Points in Elastodynamics*, *Physical Review Applied* **13**, (2020).
- [15] Y. Fang, T. Kottos, and R. Thevamaran, *Universal Route for the Emergence of Exceptional Points in PT-Symmetric Metamaterials with Unfolding Spectral Symmetries*, *New Journal of Physics* (2021).
- [16] B. Lustig, G. Elbaz, A. Muhafra, and G. Shmuel, *Anomalous Energy Transport in Laminates with Exceptional Points*, *Journal of the Mechanics and Physics of Solids* **133**, 103719 (2019).
- [17] M. I. N. Rosa, M. Mazzotti, and M. Ruzzene, *Exceptional Points and Enhanced Sensitivity in PT-Symmetric Continuous Elastic Media*, *Journal of the Mechanics and Physics of Solids* **149**, 104325 (2021).
- [18] A. Guo, G. J. Salamo, D. Duchesne, R. Morandotti, M. Volatier-Ravat, V. Aimez, G. A. Siviloglou, and D. N. Christodoulides, *Observation of PT-Symmetry Breaking in Complex Optical Potentials*, *Phys. Rev. Lett.* **103**, 93902 (2009).
- [19] Z. Lin, H. Ramezani, T. Eichelkraut, T. Kottos, H. Cao, and D. N. Christodoulides, *Unidirectional Invisibility Induced by PT-Symmetric Periodic Structures*, *Physical Review Letters* **106**, 1 (2011).
- [20] H. Hodaei, M. A. Miri, M. Heinrich, D. N. Christodoulides, and M. Khajavikhan, *Parity-Time-Symmetric Microring Lasers*, *Science* (1979) **346**, (2014).
- [21] L. Feng, Z. J. Wong, R. M. Ma, Y. Wang, and X. Zhang, *Single-Mode Laser by Parity-Time Symmetry Breaking*, *Science* (1979) **346**, (2014).
- [22] H. Hodaei, A. U. Hassan, S. Wittek, H. Garcia-Gracia, R. El-Ganainy, D. N. Christodoulides, and M. Khajavikhan, *Enhanced Sensitivity at Higher-Order Exceptional Points*, *Nature* **548**, 187 (2017).
- [23] W. Chen, Ş. Kaya Özdemir, G. Zhao, J. Wiersig, and L. Yang, *Exceptional Points Enhance Sensing in an Optical Microcavity*, *Nature* **548**, 192 (2017).
- [24] Y. H. Lai, Y. K. Lu, M. G. Suh, Z. Yuan, and K. Vahala, *Observation of the Exceptional-Point-Enhanced Sagnac Effect*, *Nature* **576**, 65 (2019).
- [25] M. P. Hokmabadi, A. Schumer, D. N. Christodoulides, and M. Khajavikhan, *Non-Hermitian Ring Laser Gyroscopes with Enhanced Sagnac Sensitivity*, *Nature* **576**, 70 (2019).
- [26] Z. Lin, A. Pick, M. Lončar, and A. W. Rodriguez, *Enhanced Spontaneous Emission at Third-Order Dirac Exceptional Points in Inverse-Designed Photonic Crystals*, *Physical Review Letters* **117**, (2016).
- [27] A. Pick, B. Zhen, O. D. Miller, C. W. Hsu, F. Hernandez, A. W. Rodriguez, M. Soljačić, and S. G. Johnson, *General Theory of Spontaneous Emission near Exceptional Points*, *Optics Express* **25**, 12325 (2017).
- [28] A. Pick, Z. Lin, W. Jin, and A. W. Rodriguez, *Enhanced Nonlinear Frequency Conversion and Purcell Enhancement at Exceptional Points*, *Physical Review B* **96**, (2017).
- [29] J. Ren, S. Franke, and S. Hughes, *Quasinormal Modes, Local Density of States, and Classical Purcell Factors for Coupled Loss-Gain Resonators*, *Physical Review X* **11**, (2021).
- [30] S. Franke, J. Ren, M. Richter, A. Knorr, and S. Hughes, *Fermi's Golden Rule for Spontaneous Emission in Absorptive and Amplifying Media*, *Physical Review Letters* **127**, (2021).
- [31] Q. Zhong, A. Hashemi, K. Özdemir, and R. El-Ganainy, *Control of Spontaneous Emission Dynamics in Microcavities with Chiral Exceptional Surfaces*, *Physical Review Research* **3**, (2021).
- [32] M. Khanbekyan and J. Wiersig, *Decay Suppression of Spontaneous Emission of a Single Emitter in a High-Q Cavity at Exceptional Points*, *Physical Review Research* **2**, (2020).
- [33] E. M. Purcell, H. C. Torrey, and R. v. Pound, *Resonance Absorption by Nuclear Magnetic Moments in a Solid*, *Physical Review* **69**, (1946).
- [34] P. A. M. Dirac, *The Quantum Theory of the Emission and Absorption of Radiation*, *Proceedings of the Royal Society of London. Series A, Containing Papers of a Mathematical and Physical Character* **114**, (1927).
- [35] E. Betzig and R. J. Chichester, *Single Molecules Observed by Near-Field Scanning Optical Microscopy*, *Science* (1979) **262**, (1993).
- [36] T. H. Taminiau, F. D. Stefani, F. B. Segerink, and N. F. van Hulst, *Optical Antennas Direct Single-Molecule Emission*, *Nature Photonics* **2**, (2008).

- [37] P. Mühlischlegel, H.-J. Eisler, O. J. F. Martin, B. Hecht, and D. W. Pohl, *Resonant Optical Antennas*, Science (1979) **308**, (2005).
- [38] M. Khajavikhan, A. Simic, M. Katz, J. H. Lee, B. Slutsky, A. Mizrahi, V. Lomakin, and Y. Fainman, *Thresholdless Nanoscale Coaxial Lasers*, Nature **482**, (2012).
- [39] R. F. Oulton, V. J. Sorger, T. Zentgraf, R. M. Ma, C. Gladden, L. Dai, G. Bartal, and X. Zhang, *Plasmon Lasers at Deep Subwavelength Scale*, Nature **461**, (2009).
- [40] J. T. Choy, B. J. M. Hausmann, T. M. Babinec, I. Bulu, M. Khan, P. Maletinsky, A. Yacoby, and M. Loñar, *Enhanced Single-Photon Emission from a Diamond-Silver Aperture*, Nature Photonics **5**, (2011).
- [41] M. Landi, J. Zhao, W. E. Prather, Y. Wu, and L. Zhang, *Acoustic Purcell Effect for Enhanced Emission*, Physical Review Letters **120**, (2018).
- [42] M. K. Schmidt, L. G. Helt, C. G. Poulton, and M. J. Steel, *Elastic Purcell Effect*, Physical Review Letters **121**, (2018).
- [43] C. Henricksen, *Loudspeakers, Enclosures, and Headphones*, Handbook for Sound Engineers **497** (1987).
- [44] M. Fink, F. Lemoult, J. de Rosny, A. Tourin, and G. Lerosey, *Subwavelength Focussing in Metamaterials Using Far Field Time Reversal*, In Acoustic Metamaterials. Springer, Dordrecht (2013).
- [45] See Supplementary Material for Additional Information about Materials and Methods.
- [46] R. S. Lakes, *Viscoelastic Solids* (2017).
- [47] E. Broitman, *Indentation Hardness Measurements at Macro-, Micro-, and Nanoscale: A Critical Overview*, Tribology Letters **65**, (2017).

**Acknowledgements:** RT and AG acknowledge the financial support from the Solid Mechanics Program of the Army Research Office (ARO) (Award No.: W911NF2010160) and the Dynamics, Control, and System Diagnostics (DCSD) Program of the National Science Foundation (NSF) (Award No.: NSF-CMMI-1925530). TK and AK acknowledge the financial support from the DCSD Program of the NSF (Award No.: NSF-CMMI-1925543) and from the Simons Foundation for Collaboration in MPS grant No 733698. We also acknowledge the assistance of Dr. Jizhe Cai on PDMS sample fabrication.

# Supplementary Materials for

## Boosting of Purcell Enhancement Factor near Exceptional Point Degeneracies in an Elastodynamic Metamaterial

Abhishek Gupta<sup>1</sup>, Arkady Kurnosov<sup>2</sup>, Tsampikos Kottos<sup>2,#</sup>, Ramathanan Thevamaran<sup>1,3,\*</sup>

<sup>1</sup>Department of Mechanical Engineering, University of Wisconsin Madison; Madison, Wisconsin, 53706, USA.

<sup>2</sup>Wave Transport in Complex Systems Lab, Physics Department, Wesleyan University; Middletown, CT-06459, USA.

<sup>3</sup>Department of Engineering Physics, University of Wisconsin Madison; Madison, Wisconsin, 53706, USA.

Correspondence to: # [tktos@wesleyan.edu](mailto:tktos@wesleyan.edu), \* [thevamaran@wisc.edu](mailto:thevamaran@wisc.edu)

### METHODS

**Experimental Methods for Spectral Measurements.** We have used the same setup that we used for the DMA measurement of the PDMS for spectral measurements of the non-Hermitian metamaterial. The non-Hermitian metamaterial is supported by a low-friction Teflon surface and a static precompression equivalent to the one used for measuring the storage and loss moduli of PDMS is applied. Since PDMS is slightly nonlinear, the precompression of PDMS should be consistent so that the storage and loss moduli remain the same as the one used for numerical modeling. A sinusoidal actuation of constant displacement amplitude at driving frequencies ranging from 10 Hz to 1200 Hz, was applied on the left side of the non-Hermitian metamaterial, and the steady-state emitted force amplitude was measured at the fixed right end. The coupling stiffness between the resonators was varied by changing the coupling springs. A sharp resonant peak is observed in the reaction-force frequency spectrum for low coupling, see Fig. 3C. As the coupling increases, the single sharp peak splits into two broad damped peaks, indicating the departure from an EPD. The peak position (real part of frequencies) and linewidth (imaginary part of frequencies) were extracted via a modal curve-fitting of the experimental data.

**Evaluation of the storage and loss moduli for the dispersionless model.** In the dispersionless approximation, the storage and loss moduli of the damped spring (PDMS) were assumed to be frequency independent. The storage modulus is approximated to be  $E' = \frac{h}{A}k_1 = 4.675MPa$ , to match the real part of stiffness of the damped spring with the undamped spring. The dispersionless complex stiffness ( $k_2$ ) is given by  $k_2 = (E' + iE'')\frac{A}{h} = E'(1 + i \tan(\delta))\frac{A}{h}$ , where  $\tan(\delta) = E''/E'$  is the dispersionless loss tangent of the damped spring. The value of  $\tan(\delta) \approx 0.326$  has been chosen such that the EPD forms at the same coupling as in dispersive model i.e.,  $\kappa_{ep} = 10.95 N/mm$ . Using this information, we have evaluated the loss moduli to be  $E'' = 1.5235MPa$ .

**Error bars calculations.** We estimated maximum variation in measurements of  $k_1$  ( $\Delta k_1$ ) and  $k_2$  ( $\Delta k_2$ ) and calculated the resultant errors in the resonant frequencies ( $\omega_+$ ,  $\omega_-$ ) using the relation

$$\Delta\omega_{\pm} = \frac{1}{2m\omega_{\pm}} \frac{\Delta k_2(m\omega_{\pm}^2 - \kappa - k_1) + \Delta k_1(m\omega_{\pm}^2 - \kappa - k_2)}{(2m\omega_{\pm}^2 - 2\kappa - k_1 - k_2)}.$$

**Spectral properties of the elastodynamic metamaterial under dispersionless approximation.**

We have found that a good description of the experimental data is obtained by considering that the storage and loss moduli take a constant value in the frequency range of our experiment (dispersionless approximation). Specifically, we have evaluated these two quantities at frequency  $\omega_* \approx 700\text{Hz}$  such that  $E'(\omega_*) \equiv k_1 h/A$ . In this case, the corresponding  $E' \approx 4.67\text{MPa}$  while  $E'' \approx E''(\omega_*) = 1.50\text{MPa}$ . Under this approximation we have that  $k_2 = (A/h) [E' + iE'']$  and the resonant frequencies  $\omega_{\pm} = \omega_{\pm}^R + i\omega_{\pm}^I$  of the system of Eqs. (2) are the solutions of the secular equation

$$[\omega_{\pm}^2 - \omega_0^2 - (\kappa/m)][\omega_{\pm}^2 - \omega_0^2 - (\kappa/m) + 2i\Gamma\omega_0] - (\kappa/m)^2 = 0. \quad (8)$$

Our experiment operates in the domain of  $\kappa \geq \kappa_{EP} \equiv m\Gamma\omega_0$  where the solutions of Eq. (8) take the form

$$\omega_{\pm}^R = \left( \left[ \omega_0^2 + (\kappa/m) \pm \sqrt{(\kappa/m)^2 - \Gamma^2\omega_0^2} \right]^2 + \Gamma^2\omega^2 \right)^{1/4} \cos(\varphi/2), \quad (9a)$$

$$\omega_{\pm}^I = \left( \left[ \omega_0^2 + (\kappa/m) \pm \sqrt{(\kappa/m)^2 - \Gamma^2\omega_0^2} \right]^2 + \Gamma^2\omega^2 \right)^{1/4} \sin(\varphi/2), \quad (9b)$$

$$\tan \varphi = \frac{\omega_0\Gamma}{\omega_0^2 + (\kappa/m) \pm \sqrt{(\kappa/m)^2 - \Gamma^2\omega_0^2}}, \quad (9c)$$

indicating that for  $\kappa = \kappa_{EP}$ , the modes are degenerate (exceptional point degeneracy). We have further confirmed the formation of an EPD by analyzing the corresponding eigenvectors. These are given by the following expression

$$\Psi_{\mp} = \frac{1}{\sqrt{2}} \left( \frac{\kappa}{m} \right)^{-1} \begin{bmatrix} -i\Gamma\omega_0 \mp \sqrt{(\kappa/m)^2 - \Gamma^2\omega_0^2} \\ (\kappa/m) \end{bmatrix}, \quad (9d)$$

demonstrating a degeneracy at  $\kappa_{EP} = m\Gamma\omega_0$ .

Further progress can be made by realizing that  $\tan \varphi \ll 1$ . The latter inequality is imposed by the physical conditions  $\omega_0\Gamma \leq (\kappa/m) \ll \omega_0^2$ ,  $\Gamma \ll \omega_0$  which dictate our experimental set-up. Using these conditions, we can simplify Eqs. (9) to the following forms

$$\omega_{\pm}^R \approx \omega_0 \left[ 1 + (\kappa/k_1) \pm \sqrt{(\kappa/k_1)^2 - (\Gamma/\omega_0)^2} \right]^{1/2}, \quad (10a)$$

$$\omega_{\pm}^I \approx \frac{1}{2} \frac{\Gamma}{\left[ 1 + (\kappa/k_1) \pm \sqrt{(\kappa/k_1)^2 - (\Gamma/\omega_0)^2} \right]^{1/2}}, \quad (10b)$$

Let us first evaluate the eigenfrequencies of the metamaterial in the limit of  $(\Gamma/\omega_0) \ll (\kappa/k_1) \ll 1$  where the last inequality always applies in our experiments. From Eqs. (10) we get that  $\omega_{\pm}^R \approx \omega_0$  and  $\omega_{\pm}^I \approx \omega_0 \sqrt{1 + 2(\kappa/k_1)}$  while for the linewidths we have  $\omega_{\pm}^I \approx \frac{1}{2}\Gamma(1 + \mathcal{O}(\frac{\kappa}{k_1}))$ . From the same equations we find that when  $(\kappa/k_1) = (\Gamma/\omega_0)$  (corresponding to stiffness

$\kappa_{EP} = m\omega_0\Gamma = \frac{A}{2h}E''$ ) the eigenvalues become degenerate (see discussion above). Notice that the condition  $(\kappa/m) = \omega_0\Gamma$  is equivalent to the relation  $(\kappa/k_1) = (\Gamma/\omega_0)$ . At EPD the eigenfrequencies Eqs. (9a,b) of the metamaterial can be simplified using Eqs. (10) to

$$\omega_{\pm}^R|_{EP} = \omega_{EP} \approx \omega_0 \left[1 + \frac{\Gamma}{\omega_0}\right]^{1/2} \approx \omega_0, \quad (10c)$$

$$\omega_{\pm}^I|_{EP} \approx \frac{1}{2} \frac{\Gamma}{[1 + (\Gamma/\omega_0)]^{1/2}} \approx \frac{\Gamma}{2}, \quad (10d)$$

where for the right-hand side of Eq. (10a,b) we have used the physical constraint that  $(\kappa/m) \ll \omega_0^2 \rightarrow \kappa/k_1 \ll 1$ . We have also confirmed that the same EPD condition is applicable for the case of eigenvectors of the couple mass system of Eqs. (2). Specifically, Eq. (9d) becomes  $\psi_+ = \psi_- = \frac{1}{\sqrt{2}} \begin{bmatrix} -i \\ 1 \end{bmatrix}$  indicating a relative phase of  $\frac{\pi}{2}$  between the two components of the degenerate eigenvector.

The validity of these approximations has been checked against the numerical results presented in the main text that have considered the dispersion characteristics of the storage and loss moduli. The comparison is shown in Extended Data Fig. 1 where we report  $\omega_{\pm}^{R,I}$ , versus the stiffness  $\kappa$ , using the approximate expressions of Eqs. (10) together with the outcomes of the exact numerics and the measurements. It is also noteworthy that, strictly speaking, due to dispersion effects, our designed metamaterial shows a quasi-EPD degeneracy. Nevertheless, for all practical purposes this quasi-degeneracy is sufficient for observing all novel features characterizing systems with EPD.

**General expression for dissipated power:** The averaged (over one driving cycle) dissipated power is given by the expression (29)

$$P_d(\omega) = \frac{\omega}{2\pi} W_d = Ah \frac{\omega}{2\pi} \int_0^{2\pi/\omega} dt \sigma(t) \frac{d\epsilon}{dt}, \quad (11)$$

where  $W_d$  is the dissipated energy per cycle. This choice of definition guaranties that the elastic component will not contribute to the final calculation since the work done by conservative forces is zero along a close loop. For the evaluation of  $P_d(\omega)$  we use the following relations

$$\epsilon(t) = |\epsilon(\omega)| \sin \omega t, \quad \sigma(t) = |\sigma(\omega)| \sin(\omega t + \delta), \quad \sin\delta(\omega) = \frac{E''(\omega)}{\sqrt{|E'(\omega)|^2 + |E''(\omega)|^2}}, \quad (12)$$

where we have also introduced the loss-tangent  $\tan\delta(\omega) \equiv E''(\omega)/E'(\omega)$ . These equations allow us to express Eq. (11) in the form

$$\begin{aligned} P_d(\omega) &= Ah \frac{\omega}{2\pi} |\epsilon(\omega)|^2 \sqrt{|E'|^2 + |E''|^2} \int_0^{2\pi/\omega} \omega \sin(\omega t + \delta) \cos \omega t \, dt \\ &= Ah \frac{\omega}{2} E''(\omega) |\epsilon(\omega)|^2 = \frac{\omega}{2h} A E''(\omega) |x_2(\omega)|^2, \end{aligned} \quad (13)$$

where we used the stress-strain relation in the frequency domain  $\sigma(\omega) = [E'(\omega) + iE''(\omega)]\epsilon(\omega)$  and the fact that  $\epsilon(\omega) = x_2(\omega)/h$ .

Therefore, the task at hand is to evaluate the displacement of the second mass  $x_2(\omega)$  and by substituting in Eq. (13) evaluate the average dissipated power  $P_d(\omega)$ . To this end, we rewrite Eqs. (2) in a matrix form as

$$(\hat{J}\omega^2 - \hat{L})\psi = s \quad (14)$$

where

$$\hat{\mathcal{L}}(\omega) = \begin{bmatrix} \frac{k_1}{m} + \frac{\kappa}{m} & \frac{\kappa}{m} \\ \frac{\kappa}{m} & \frac{A}{mh} E'(\omega) + \frac{\kappa}{m} + i \frac{A}{mh} E''(\omega) \end{bmatrix}, \quad \psi = \begin{bmatrix} x_1(\omega) \\ x_2(\omega) \end{bmatrix}, \quad s = \begin{bmatrix} -\frac{k_1}{m} U \\ 0 \end{bmatrix} \quad (15)$$

and  $\hat{\mathcal{J}}$  is the identity  $2 \times 2$  matrix. The solution of Eq. (14) is then

$$\psi = \hat{\mathcal{G}}s; \quad \hat{\mathcal{G}} = \frac{1}{\det(\hat{\mathcal{J}}\omega^2 - \hat{\mathcal{L}})} \begin{bmatrix} \omega^2 - \frac{A}{mh} E'(\omega) - \frac{\kappa}{m} - i \frac{A}{mh} E''(\omega) & -\frac{\kappa}{m} \\ -\frac{\kappa}{m} & \omega^2 - \frac{k_1}{m} - \frac{\kappa}{m} \end{bmatrix}, \quad (16)$$

where  $\hat{\mathcal{G}} \equiv (\hat{\mathcal{J}}\omega^2 - \hat{\mathcal{L}})^{-1}$  is the Green's function that describes the dynamics of the metamaterial. Consequently, the displacement  $x_2(\omega)$  becomes

$$|x_2(\omega)|^2 = \left| (\hat{\mathcal{G}}s)_2 \right|^2 = |G_{21}|^2 |s_1|^2 = \frac{(\kappa/m)^2 (k_1/m)^2 |U|^2}{|\det(\hat{\mathcal{J}}\omega^2 - \hat{\mathcal{L}})|^2}, \quad (17)$$

It could be shown that  $|\det(\hat{\mathcal{J}}\omega^2 - \hat{\mathcal{L}})|^2 \text{Im} G_{11} = \frac{A}{mh} E''(\omega) \left(\frac{\kappa}{m}\right)^2$  which allows us to establish the following important equality between matrix elements of the Green's function

$$\text{Im}(G_{11}) = \frac{A}{mh} E''(\omega) |G_{21}|^2. \quad (18)$$

Combining Eqs. (13,17,18), we finally get that the dissipation power can be expressed as in Eq. (3) where  $\xi(\omega) = \frac{2\omega}{\pi} \text{Im} G_{11}$  has dimensions of density of states.

## SUPPLEMENTARY TEXT

### LDoS Analysis in the two limiting cases [Eq. (5) and Eq. (6) of the main text]

Using the definition of  $\xi(\omega) = \frac{2\omega}{\pi} \text{Im} G_{11}(\omega)$  from Eq. (3) of the main text and the expression for the Green's function of the metamaterial (see Eq. (16) of the main text), we can now deduce Eq. (4) of the main text. Specifically,  $\xi(\omega)$  takes the form

$$\xi(\omega) = \frac{1}{\pi} \frac{\Gamma\omega_0(\kappa/m)^2\omega}{[\omega^2 - \omega_0^2]^2 [\omega^2 - \omega_0^2 - 2(\kappa/m)]^2 + (2\Gamma\omega_0)^2 [\omega^2 - \omega_0^2 - (\kappa/m)]^2}. \quad (S1)$$

The two limiting cases corresponding to the shape of  $\xi(\omega)$  in the proximity of an EPD and far away from it can be deduced from Eq. (S1).

**1. Proximity to the EPD:** The EPD occurs at  $\kappa_{EP}/m = \Gamma\omega_0 \rightarrow \kappa_{EP} = \frac{A}{2h} E''$  leading to a degenerate resonant frequency  $\omega_{\pm}^R = \omega_{EP} = \omega_0 \sqrt{1 + \Gamma/\omega_0}$  (see Eq. 10a of the main text). Straightforward algebra allows us to rewrite the denominator of Eq. (S1) in a simpler form, leading to the following expression for  $\xi(\omega)$ :

$$\xi_{EP}(\omega) = \frac{1}{\pi} \frac{(\Gamma\omega_0)^3 \omega}{[(\omega^2 - \omega_{EP}^2)^2 + (\Gamma\omega_0)^2]^2} \quad (S2)$$

At the vicinity of  $\omega \simeq \omega_{EP}$ , the DoS can be further approximated as

$$\xi_{EP}(\omega \simeq \omega_{EP}) \approx \frac{1}{\pi} \frac{(\Gamma\omega_0)^3 \omega_{EP}}{[4\omega_{EP}^2(\omega - \omega_{EP})^2 + (\Gamma\omega_0)^2]^2} \approx \frac{1}{2\pi} \frac{(\Gamma/2)^3}{[(\omega - \omega_{EP})^2 + (\Gamma/2)^2]^2} \quad (S3)$$

where in the last step, we have assumed that  $\omega_{EP} = \omega_0 \sqrt{1 + \Gamma/\omega_0} = \omega_0 [1 + \mathcal{O}(\Gamma/\omega_0)] \approx \omega_0$ . The last expression in Eq. (S3) is equal to the expression of Eq. (5) of the main text.

**2. Limit of  $(\kappa/m) \gg \Gamma\omega_0$ :** In this case the resonant frequencies are at positions  $\omega_-^R \approx \omega_0$  and  $\omega_+^R \approx \sqrt{\omega_0^2 + 2(\kappa/m)}$  (see discussion above Eq. (10) of main text). In the vicinity of  $\omega_- = \omega_0$  the denominator of Eq. (S1) can be further simplified leading to the following expression for the DoS:

$$\xi_\infty(\omega \approx \omega_-^R) \approx \frac{1}{8\pi} \frac{\Gamma/2}{(\omega - \omega_-^R)^2 + (\Gamma/2)^2} \quad (S4)$$

Similarly, in the vicinity of  $\omega_+^R = \sqrt{\omega_0^2 + 2(\kappa/m)}$ , the denominator of Eq. (S1) can be further simplified leading to the following expression for the DoS:

$$\xi_\infty(\omega \approx \omega_+^R) \approx \frac{1}{8\pi} \frac{\Gamma/2}{(\omega - \omega_+^R)^2 + (\Gamma/2)^2}, \quad (S5)$$

which is valid under the constraint that  $(\kappa/k_1) \ll 1$ .

Combining Eqs. (S4,S5) we can come up with the approximate description Eq. (6) of the LDoS in all frequency range when  $\kappa \gg \kappa_{EP}$ . Using the results of Eqs. (S3,S5) we can evaluate the ratio  $\mathcal{P}(\omega_e = \omega_{EP}) = 4$ .

A more detailed analysis can reveal small deviations from the four-fold enhancement of  $\mathcal{P}(\omega_e = \omega_{EP}) = \frac{\xi_{EP}(\omega_{EP})}{\xi_\infty(\omega_+^R)}$ . Specifically from Eq. (S2), when it is evaluated at EPD we get

$$\xi_{EP}(\omega_{EP}) = \frac{1}{\pi\Gamma} \sqrt{1 + \frac{\Gamma}{\omega_0}} \approx \frac{1}{\pi\Gamma} \left(1 + \frac{1}{2} \frac{\Gamma}{\omega_0}\right) + \mathcal{O}\left(\left(\frac{\Gamma}{\omega_0}\right)^2\right); \quad (S6)$$

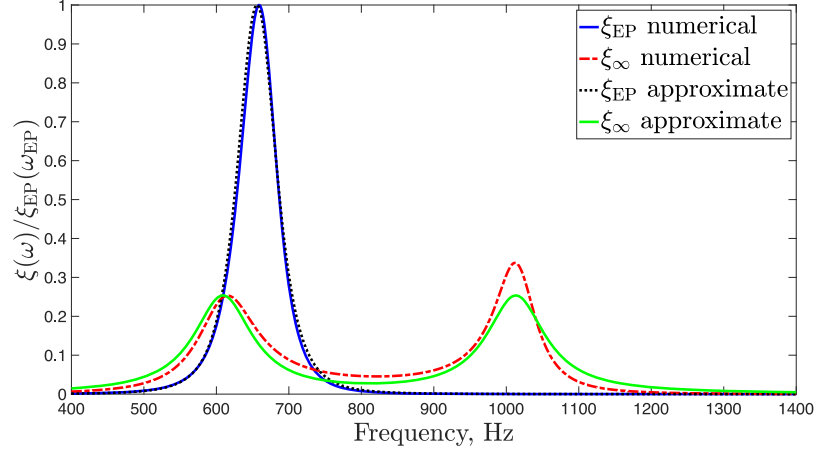
In a similar manner, we evaluate  $\xi_\infty(\omega_+^R)$  using Eq. (S1). Specifically, by substituting the value  $\omega_+^R = \sqrt{\omega_0^2 + 2(\kappa/m)}$  in this expression, we get

$$\xi_\infty(\omega_+^R) = \frac{1}{4\pi\Gamma} \sqrt{1 + \frac{2\kappa}{k_1}} \approx \frac{1}{4\pi\Gamma} \left(1 + \frac{\kappa}{k_1}\right) + \mathcal{O}\left(\left(\frac{\kappa}{k_1}\right)^2\right); \quad (S7)$$

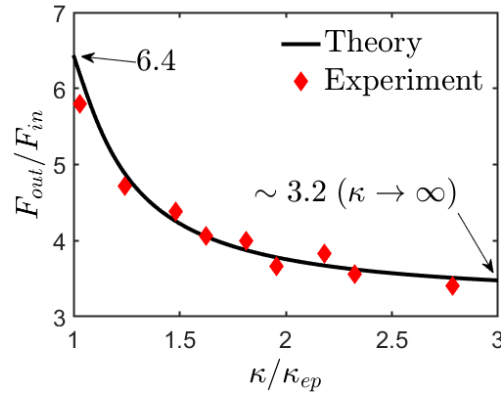
Taking the ratio between Eqs. (S6,S7), we finally get

$$\mathcal{P}(\omega_e = \omega_{EP}) \approx 4 \frac{\left(1 + \frac{1}{2} \frac{\Gamma}{\omega_0}\right)}{\left(1 + \frac{\kappa}{k_1}\right)} \approx 4 \left(1 - \frac{\kappa}{k_1} + \frac{1}{2} \frac{\Gamma}{\omega_0}\right); \quad (S8)$$

The validity of the above approximations has been confirmed numerically by comparing the expressions in Eqs. (5, 6) of the main text with the exact numerical results of  $\xi(\omega)$  for our metamaterial. In these simulations, the value of  $x_2(\omega)$  from Eq. (13) of the main text, has been evaluated using the dispersion characteristics of the dynamic modulus. The numerical results together with the theory is shown in Fig. S1.



**Supplementary Fig. S1. The LDoS function  $\xi(\omega)$  versus frequency.** Two representative cases corresponding to spring stiffness of  $\kappa = \kappa_{EP} = 10.95 \text{ kN/m}$  (dashed black and solid blue lines) and  $\kappa = \kappa_{\infty} = 60 \text{ kN/m}$  (dashed red and solid green lines). The green and blue solid lines correspond to the approximate expressions Eq. (S3) and Eq. (6) of the main text. The red dashed-dotted and black dashed lines correspond to the numerical evaluation of  $\xi(\omega)$  via Eq. (2) where the dispersion characteristics of  $E'(\omega)$  and  $E''(\omega)$  are taken into consideration. The parameters used in the plot are  $k_1 = 67.87 \text{ kN/m}$ ,  $h = 1.95 \text{ mm}$ ,  $A = 28.3 \text{ mm}^2$ ,  $m = 4.6 \text{ g}$ , and  $\omega_0 = \sqrt{k_1/m} = 2\pi \times 609 \text{ rad/s}$ . In the case of dispersionless modeling  $E' = k_1 h/A = 4.67 \text{ MPa}$  and  $E'' = 1.50 \text{ MPa}$  while the critical coupling has been estimated to be  $\kappa_{EP} = 10.95 \text{ kN/m}$ . All the data are normalized by the maximum value  $\xi_{EP}(\omega_{EP})$ . The slightly larger deviation of the approximate result Eq. (6) (green solid line) from the numerical data (red dash-dotted line) at the higher frequency  $\omega_+$  is expected because the ratio  $(\kappa/k_1) = 0.88$  is barely satisfying the condition  $\kappa/k_1 < 1$  for the chosen  $\kappa_{\infty} = 60 \text{ kN/m}$ .



**Supplementary Fig. S2. Boosting of Purcell Enhancement factor.** The actuation force enhancement of 3.2 due to Purcell effect is observed when the metamaterial is far from EPD, which is boosted to 6.4 when the system is at the proximity to EPD.